Global and Planetary Change 125 (2015) 1–12

Contents lists available at ScienceDirect

Global and Planetary Change

journal homepage: www.elsevier.com/locate/gloplacha

Rapid longitudinal migrations of the filament front off Namibia (SE Atlantic) during the past 70 kyr

O.E. Romero [a,*], X. Crosta [b], J.-H. Kim [c], L. Pichevin [d], J. Crespin [b]

[a] MARUM — Center for Marine Environmental Sciences, University of Bremen, Leobener Str., 28359 Bremen, Germany
[b] CNRS/INSU, UMR5805, EPOC, Université Bordeaux 1, Talence Cedex, France
[c] NIOZ Royal Netherlands Institute for Sea Research, NL-1790 AB Den Burg, The Netherlands
[d] School of Geosciences, Grant Institute, University of Edinburgh, West Main Road, EH10 3JW, Edinburgh, UK

ARTICLE INFO

Article history:
Received 15 May 2014
Received in revised form 20 November 2014
Accepted 3 December 2014
Available online 8 December 2014

Keywords:
Benguela
Diatoms
Millennial and submillennial time scale
Productivity
Sea-surface temperature
SW Atlantic
Upwelling filaments

ABSTRACT

Although productivity variations in coastal upwelling areas are mostly attributed to changes in wind strength, productivity dynamics in the Benguela Upwelling System (BUS) is less straightforward due to its complex atmospheric and hydrographic settings. In view of these settings, past productivity variations in the BUS can be better investigated with downcore sediments representing different productivity regimes. In this study, two sediment cores retrieved at ca. 25°–26°S in the BUS and representing different productivity regimes were studied. By using micropaleontological, geochemical and temperature proxies measured on core MD96-2098, recovered at 2910 m water depth in the bathypelagic zone at 26°S off Namibia, variations of filament front location, productivity and temperature in the central BUS over the past 70 kyr were reconstructed. The comparison with newly-generated alkenone-based sea-surface temperature (SST) and previously obtained data at site GeoB3606-1 (~25°S; ca. 50 km shoreward from MD96-2098) allowed the recognition of four main phases: (1) upwelling front above the mid slope (70 kyr–44 kyr), (2) seaward displacement of the upwelling front beyond the mid slope (44 kyr–31 kyr), (3) main upwelling front over the hemipelagial (31 kyr–19 kyr), and (4) shoreward contraction of the upwelling filament, and decreased upwelling strength over most of the uppermost bathypelagic (19 kyr–6 kyr). The latitudinal migration of the Southern Hemisphere westerlies and the consequent contractions and expansions of the subpolar gyre played a significant role in millennial and submillennial variability of SST off Namibia. The strength of the southeasterly trade winds, rapid sea-level variations and the equatorward leakage of Antarctic silicate might have acted as amplifiers. Although late Quaternary variations of productivity and upwelling intensity in eastern boundary current systems are thought to be primarily linked to the variability in wind stress, this multi-parameter reconstruction shows that interplaying mechanisms defined the temporal variation pattern of the filament front migrations and the diatom production off Namibia during the past 70 kyr.

1. Introduction

Due to intense upwelling and strong nutrient recycling, primary productivity variations of eastern boundary current systems play a significant role in regulating the present-day CO_2 content of the atmosphere (Longhurst et al., 1995). Among these high productive marine coastal areas, the Benguela Upwelling System (BUS) along SW Africa is spatially one of the present-day largest systems (Shannon, 1985). The BUS exhibits a range of filaments (narrow protuberances extending from main upwelling zone, see below Section 2) and frontal meanders that represent an effective mechanism for nutrient export from the productive inner shelf to the less nutrient-rich pelagic realm (Shillington, 1998). The spatial area covered by filaments along the South African and Namibian coast is more extensive than that of the proper coastal upwelling (Lutjeharms and Stockton, 1987). The up-to-750 km seaward transport of nutrients and microorganisms affects the dynamics and the intensity of the primary productivity over most of the continental slope and the pelagic Atlantic off SW Africa (Shillington, 1998). Hence, it is conceivable that a substantial or even a major portion of the total primary production attributable to the upwelling dynamics takes place in the filaments and not along the coastal upwelling region (Lutjeharms and Stockton, 1987).

As known from similar coastal upwelling settings (*e.g.*, off NW Africa and off Peru; Romero et al., 2008; Romero and Armand, 2010), the current heterogeneous spatial distribution of nutrients in the BUS causes a marked east-west primary productivity gradient off SW Africa (Shannon, 1985; Lutjeharms and Stockton, 1987). Due to the strong spatial heterogeneity of hydrography and atmospheric conditions off SW Africa, generalized statements on paleoproductivity based on only one core location have proven to be insufficient (Mollenhauer et al., 2002). The combined effect of a productivity gradient and increasing

* Corresponding author.
E-mail address: oromero@uni-bremen.de (O.E. Romero).

http://dx.doi.org/10.1016/j.gloplacha.2014.12.001
0921-8181/

water depth with increasing distance from the shoreline resulted in variable sedimentation patterns during the late Quaternary along the SW African coast (Mollenhauer et al., 2002; Pichevin et al., 2005a,b; Romero, 2010). Whether the offshore transport of nutrients from the Namibian coastal area upon the pelagic realm had any effect on the long-term paleoproductivity has still to be demonstrated.

Following the fact that modern enhanced productivity concentrates at the filament front (Lutjeharms and Stockton, 1987), we hypothesize that past variations of the front location and primary productivity intensity should be recognized in downcore sediments. By comparing micropaleontological and geochemical data from two sediment cores, we were able to reconstruct past migrations of the filament front location and assessed their effects on primary productivity over the past 70 kyr. We generated micropaleontological (diatoms) and geochemical (calcium carbonate, organic carbon, opal, $\delta^{18}O$ of benthic foraminifera, and alkenone-based sea surface temperatures (SST)) data for core MD96-2098 (off Lüderitz, Namibia, Fig. 1). These records were compared with those previously published from the nearby core GeoB3606-1 (Romero, 2010). In addition, we obtained a new submillennial-resolved alkenone SST record for core GeoB3606-1. Owing to the longitudinal geographical distance between both drill sites (ca. 26 nautical miles = ca. 50 km), the two studied core sites are located in the present-day back-and-forth migration front of one of the most productive and dynamic BUS filaments (Shannon, 1985; Lutjeharms and Stockton, 1987). Site MD96-2098 is located in the less productive zone, beyond the present-day outermost border of the filaments at 26°–25°S off Lüderitz (Fig. 1), while site GeoB3606-1 is located in the middle-slope, presently mostly beneath or close to the more productive surface waters overlying the upper and middle continental slope. The comparison of the new and published data allows us to build a coherent, synoptic picture of past changes in productivity in the Lüderitz area, addressing issues such as variations in the filament extensions/contractions, the intensity of the upwelling, and the nutrient availability in the central BUS during the past 70 kyr.

2. Modern oceanographic and climatic settings

The BUS extends along the SW African margin, adjacent to the coast of Angola, Namibia and South Africa. Its northern and southern boundaries are defined as the Angola–Benguela Front and the Agulhas retroflection, respectively (Lutjeharms and Meeuwis, 1987). The present-day wind field off SW Africa is dominated by the trade winds, which cause the occurrence of upwelling in austral spring and summer off Lüderitz (Shannon and Nelson, 1996). Prevailing southeasterly trade winds drive the upwelling of cold and nutrient-rich waters originating from depths between 150 and 330 m (roughly corresponding to the South Atlantic Central Water, Shannon, 1985, and references therein).

The SE Atlantic upwelling regime consists of a spatially continuous coastal upwelling strip, as well as an offshore area consisting of several mesoscale features. Off Lüderitz (25°–26°S), these features (a collection of plumes, streamers, eddies and filaments; Lutjeharms and Stockton, 1987) exhibit a tendency to extend farther offshore than further north and further south. For this study, the term "filament" is used for narrow (<50 km) protuberances extending more than 50 km from the main thermal upwelling front and being narrower than 50 km. Such filaments occasionally coalesce to form a much wider amalgamated feature, which is hereafter referred to as an upwelling plume (Lutjeharms and Stockton, 1987). Plumes are also formed in other ways than the product of filament fusion.

Based on their spatial and temporal variability and their relationships to wind forcing, 12 main coastal upwelling cells have been identified in the upwelling regime off southern Africa's west coast (Lutjeharms and Meeuwis, 1987). Among them, the region around Lüderitz (25°–26°S, Fig. 1) region was identified already in the early 1950s as an important upwelling site (Shannon, 1985, and references therein). An analysis of present-day mean SST found in each upwelling cell shows that there exists a well-behaved, latitudinally determined, thermal relationship: mean SST decreases from north to south to the latitude of Lüderitz after which it increases monotonically southwards (Lutjeharms and Meeuwis, 1987). Along the SW African margin, the most frequent upwelling events, the furthest offshore extension of the filament, and the highest frequency of occurrence of filaments occur off Lüderitz (Lutjeharms and Meeuwis, 1987).

The thermal front off Lüderitz, coincident with the shelf break, demarcates the seaward extent of upwelled waters. This front is highly convoluted, often disturbed by small filaments and eddies, and extends seaward as far as 750 km (Lutjeharms and Meeuwis, 1987). On the offshore side of the front, secondary upwelling may occur. Since the development of the extensive and highly convoluted field of filaments,

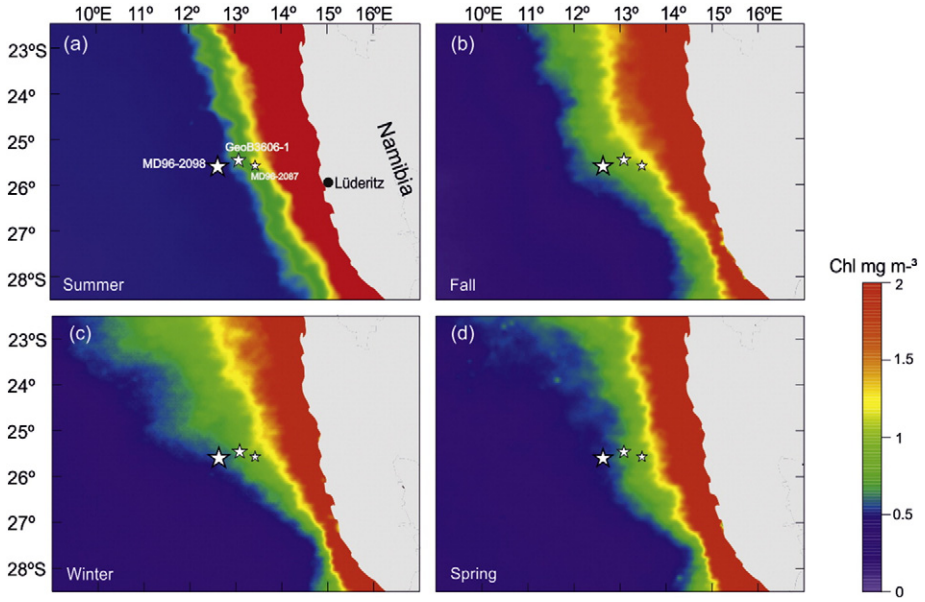

Fig. 1. Location of the study site MD96-2098 and comparison site GeoB3606-1 (white stars) in the Benguela Upwelling System. Location of core MD96-2087 is shown for comparison. Seasonally averaged concentration of chlorophyll *a* (mg m^{-3}) for (a) January–March (austral summer), (b) April–June (austral fall), (c) July–September (austral winter), and (d) October–December (austral spring) from the years 1998–2009 in 9 by 9 km resolution (Goddard Space Flight Center, http://oceancolor.gsfc.nasa.gov/SeaWiFS/)

eddies, and thermal fronts is favorable for high productivity (Shannon, 1985, and references therein), enhanced phytoplankton productivity does not often occur in the center of upwelling cells, but rather offshore and at the borders, or just outside, of upwelling centers (Lutjeharms and Stockton, 1987, and references therein). With the onset of winter the Namibia upwelling cell and the filamentous components are strongly developed (Lutjeharms and Meeuwis, 1987). Though clearly present throughout the year, the Lüderitz cell is thermally most intense during fall, broadening its alongshore extent into the Walvis area in winter and spring. This seasonal pattern is mirrored by pigment concentration in surface waters (Fig. 1).

The maximum wind stress over the Lüderitz upwelling system lies in a band offshore, which lays some 200–300 km offshore. Together with wind-stress patterns, the bottom topography possibly determines the axes angles of the upwelling system. The axis orientation observed in the upwelling filaments shows increasing trend to east-west zonality off Lüderitz (Lutjeharms and Stockton, 1987, and references therein).

3. Materials and methods

3.1. Core location

Piston core MD96-2098 (25° 35.99′ S, 12° 37.79′ E, 2910 m water depth) was collected off Namibia (Fig. 1) during Images II — NAUSICAA cruise on R/V Marion Dufresne II (Bertrand, 1997). Gravity core GeoB3606-1 (core length = 1074 cm; 25° 28.0′ S, 13° 05.0′ E; Romero, 2010) was collected on R/V METEOR cruise 34/1 from a water depth of 1785 m on the continental slope of the Cape Basin (Fig. 1).

3.2. Stratigraphy and sampling

The stratigraphy for core MD96-2098 is based on oxygen isotope analyses on shells of the benthic foraminifera *Cibicidoides wuellerstorfi* and was previously presented by Pichevin et al. (2005a). Here, we present an updated chronology by tuning the MD96-2098 $\delta^{18}O$ record to the well-dated *Globigerina inflata* $\delta^{18}O$ record from the nearby core GeoB1711-4 (12.37° S, 23.32° E; Kirst et al., 1999; Romero, 2010). Being deeper, GeoB1711-4 (water depth = ca. 1990 m) offers a better environmental constrain than GeoB3606-1 (water depth = ca. 1780 m). The last 34,000 years from core GeoB1711-4 were dated by seven AMS^{14}C measurements that were calibrated with CALIB 6 and Marine 09 calibration curve (Romero and Armand, 2010), thus giving good age constraints for the top part of the core. Beyond the radiocarbon range, the chronology of core GeoB1711-4 was done by tuning its $\delta^{18}O$ record to the $\delta^{18}O$ reference curve (Lisiecki and Raymo, 2005). The tuning between MD96-2098 and GeoB1711-4 cores bases on eight tie-points over the past 140 kyr, which were chosen because they represent well-known climatic events and are well expressed in both $\delta^{18}O$ records (Fig. 2). The core top was dated by comparing the $\delta^{18}O$ of both cores and is only a rough estimate in the absence of AMS^{14}C dates for MD96-2098. However, this estimation does not undermine our interpretations before the Holocene.

The total length of core MD96-2098 is 3224 cm. In this study, we presented results for the upper 1000 cm (6–70 kyr) except for the alkenone analysis that was performed only in the uppermost 460 cm. For the studied time interval, the sedimentation rate (SR) ranged between ~7. 0 and ~20.0 cm kyr^{-1} (Fig. 2). SR remained above 7 cm kyr^{-1} for most of the studied period and reached its highest values (20 cm kyr^{-1}) between 70 and 230 cm (18.0–10.50 kyr) (Fig. 2). Depending on the sedimentation rates, sampling resulted in temporal resolution varying between ~100 years and ~1000 years for diatom counts and bulk geochemical and isotope analyses and between ~1000 years and ~3000 years for alkenone analyses.

The age model for core GeoB3606-1 has been published elsewhere (Romero, 2010). The published conventional radiocarbon (^{14}C) ages for GeoB3606-1 were converted to calendar ages, considering the ocean average of 400-yr reservoir age (Romero, 2010). Core GeoB3606-1 was sampled every 5 cm, allowing analyses to be carried out at an average sample interval ranging between 100 years and 250 years.

3.3. Diatoms

3.3.1. Sample preparation and census of valves

Diatom slides were prepared following the protocol by Rathburn et al. (1997). Identification and counts were performed using an Olympus BH2 photomicroscope (EPOC, Talence, France) at ×1000 magnification. Three coverslips per sample were examined. Following the counting procedure described in Crosta and Koç (2007), a minimum of 300 valves per slide were identified and counted. Several traverses across each coverslip were studied, depending on the valve abundance. Diatoms were identified to species or species group level. Species identification mainly follows Sundström (1986), Moreno-Ruiz and Licea (1994), Moreno-Ruiz et al. (1996), and Hasle and Syversten (1997). The relative abundance (%) of each species was determined as the fraction of the diatom species versus the total diatom abundance in a particular sample.

Diatom accumulation rates were calculated with the following equation:

$$DAR = (Nv * WBD * SR)/2$$

where DAR is the diatom accumulation rate in millions cm^{-2} kyr^{-1}, Nv is the number of diatom valves per gram of dry sediment, WBD is the wet bulk density in g cm^{-3}, and SR is the sedimentation rates in cm kyr^{-1}.

3.3.2. Ecology of diatoms

To simplify the analysis of the paleoecological information of the diverse diatom community (ca. 40 species identified in core MD96-2098), species sharing similar ecology were lumped together. Based on habitats, nutrients and SST requirements, previous investigations on diatom distribution in surface waters and in surface sediments from low-latitude coastal and hemipelagic marine environments (Romero et al., 2002, 2005; Romero and Armand, 2010) have demonstrated that it is useful to combine diatom species in several groups to better understand paleoecological changes (*e.g.*, Romero et al., 2011, 2012; Crosta et al., 2012). The build-up of groups was based on simple comparison of relative abundances or statistical approaches.

We defined four main diatom groups: pelagic–oligotrophic, coastal planktonic, upwelling, and benthic. Marine pelagic–oligotrophic diatoms thrive in warm, nutrient-poor surface waters with low siliceous productivity. At site MD96-2098, the pelagic–oligotrophic group is mainly composed by large and well-silicified centric diatoms – such as *Azpeitia* spp., *Planktoniella sol*, *Pseudosolenia calcar-avis*, *Rhizosolenia* spp., and *Thalassiosira* spp. with lesser contribution by pennate forms such as *Nitzschia* spp. and *Thalassionema bacillaris*.

Coastal planktonic diatoms thrive in nutrient-rich coastal marine environments. This group, which tracks high dissolved silica contents, non-upwelling conditions and low turbulence waters, is composed at site MD96-2098 by several large and well silicified centric diatoms such as *Actinocyclus* spp., *Actinoptychus* spp., *Coscinodiscus* spp., and the pennate *Fragilariopsis doliolus*.

Upwelling diatoms thrive in surface waters with high dissolved silica concentrations and/or high rate of nutrient replenishment to sustain blooming conditions. At site MD96-2098, this group is dominated by resting spores *Chaetoceros* spp. and *Thalassionema nitzschioides* var. *nitzschioides*. These species are abundant in areas of coastal or front filament upwelling, though they can also reach high abundances in eutrophic environments with suitable concentrations of Si and Fe (Romero and Armand, 2010).

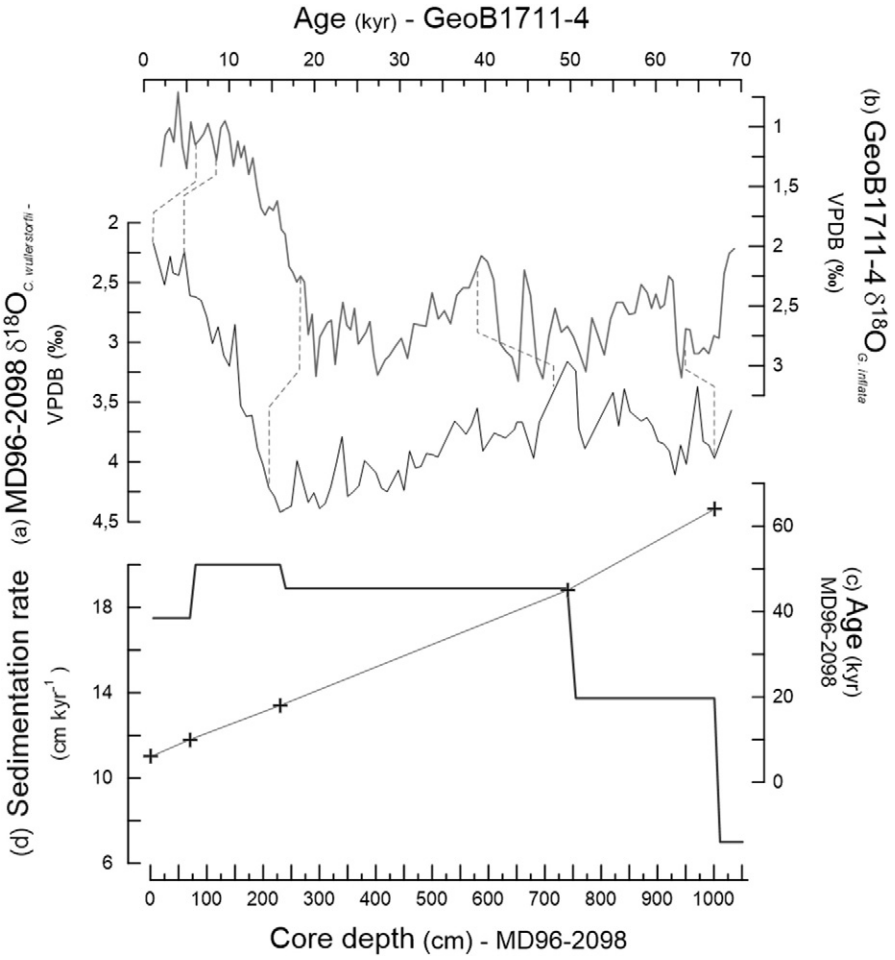

Fig. 2. Stratigraphy and sedimentation rate of Site MD96-2098. (a) Oxygen isotopes ratios (‰ VPDB) measured on the planktic foraminifera *Globigerina inflata* (GeoB1711-4, 12.37°S, 23.32°E, Kirst et al., 1999); (b) oxygen isotopes ratios (‰ VPDB) measured on the benthic foraminifera *Cibicidoides wuellerstorfi* (site MD96-2098); (c) five tie-points (black crosses) based on oxygen isotope analyses of the benthic foraminifera *Cibicidoides wuellerstorfi* (Pichevin et al., 2005a, b; revised here) and its correlation with GeoB1711-4; (d) sedimentation rate (cm^{-2} kyr^{-1}) for the past 70 kyr (upper 1050 cm of core MD96-2098). The dotted lines (upper panel) represent the tie points between GeoB1711-4 and MD96-2098.

Benthic diatoms occur attached to a substratum (rocks, sand, mudflats, macrophytes, etc.), occur predominantly in shallow (<50 m), marine to brackish waters of coastal marine zones and river mouths, and track the transport from the coast and/or river mouth towards hemipelagic and pelagic waters (Romero, 2010; Romero and Armand, 2010). At site MD96-2098, pennate diatoms (particularly marine *Cocconeis* spp.) contribute the most.

3.4. Bulk geochemical analyses

We used absorbance mid-infrared spectroscopy in transmission mode at the Museum National d'Histoire Naturelle (Paris, France) as a quantitative method to determine biogenic opal concentration in MD96-2098. In given conditions (described below), the amount of absorbed radiation is proportional to the quantity of absorbing matter in the sample (Bertaux et al., 1998). Samples for opal measurements were mechanically ground with small agate balls in an agate vial. Particle size of less than 2 mm is required to avoid excessive scattering of IR radiation. The powder then was carefully mixed with KBr in an agate mortar. A dilution of 0.25% was used for all samples studied. Pellets (300 mg, 13 mm in diameter) were prepared by pressing the mixture in a vacuum die, applying up to 8 tons cm^{-2} of compression. The pellets were oven-dried for 2 days before data acquisition. IR spectra were recorded on a Perkin-Elmer FT 16 PC spectrometer in the 4000–250 cm^{-2} energy range with a 2 cm^{-2} resolution. For each spectrum, 50 scans were cumulated. Absorbance was computed relative to a blank (pure KBr pellet). To determine biogenic opal concentration, the area of the opal absorbance peak was multiplied by its specific absorbance coefficient *k* of 0.205.

Calcium carbonate ($CaCO_3$) measurements were performed applying a gasometric method. Total organic carbon (TOC) measurements were performed on a LECO C–S 125 analyzer at EPOC (Talence, France) after treatment of the sediment with hydrochloric acid to remove $CaCO_3$. For both analyses, the precision was around 5%, expressed as the coefficient of variation of replicate determinations.

3.5. Alkenone analyses and SST estimations

The SST estimates were based on alkenone measurements. Long-chain unsaturated ketones for MD96-2098 were extracted and analysed by gas chromatography at EPOC, following the methodology described by Villanueva and Grimalt (1997). To determine past SST variations for GeoB3606-1, alkenones were extracted from 1 to 2 g portions of freeze-dried and homogenized sediment at MARUM (Bremen, Germany) following the procedure described by Kim et al. (2002). The extracts were analyzed by capillary gas chromatography using a gas chromatograph (HP 5890A) equipped with a 60 m column (J&W DB1, 0.32 mm × 0.25 μm), a split injector (1:10 split modus), and a flame ionization detector. Quantification of the alkenone content was achieved using squalane as an internal standard.

The alkenone unsaturation index U^K_{37} was calculated from $U^K_{37} = (C_{37:2})/(C_{37:2} + C_{37:3})$ as defined by Prahl and Wakeham (1987),

where $C_{37:2}$ and $C_{37:3}$ are the di- and tri-unsaturated C_{37} methyl alkenones. The U^K_{37} values were converted into temperature values applying the culture calibration of Prahl et al. (1988) ($U^K_{37} = 0.034*T + 0.039$), which has also been validated by coretop compilations (Müller et al., 1998). The precision of the measurements ($\pm 1\sigma$) was better than 0.003 U^K_{37} units (or 0.1 °C), based on multiple extractions and analyses of a sediment sample used as a laboratory internal reference from the South Atlantic.

4. Results

4.1. Diatoms

At site MD96-2098, total diatom accumulation rate ($diatom_{AR}$) ranged between 1.2×10^8 and 4.7×10^9 valves g^{-2} kyr^{-1} (average = 1.1×10^9 valves g^{-2} kyr^{-1}). Highest $diatom_{AR}$ (>2.0×10^9 valves g^{-2} kyr^{-1}) occurred at 33,5 kyr, 31–29 kyr, 27–25 kyr and during the

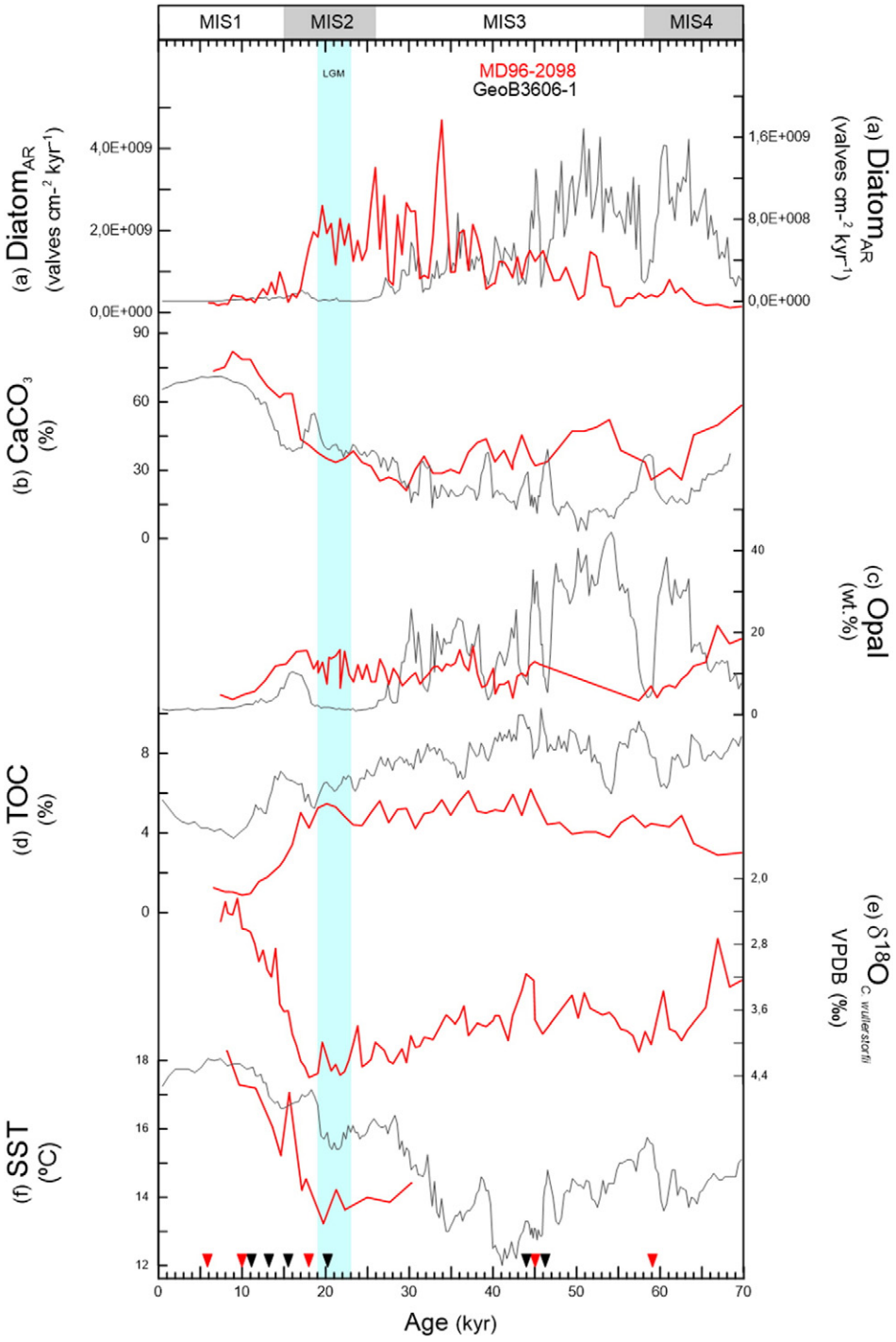

Fig. 3. Accumulation rates (AR) of (a) total diatoms (valves cm^{-2} kyr^{-1}), and concentration of (b) calcium carbonate ($CaCO_3$, %), (c) opal (wt.%), (d) total organic carbon (TOC, wt.%) in cores MD96-2098 (red line) and GeoB3606-1 (gray line), (e) oxygen isotopes ratios (‰ VPDB) measured on the benthic foraminifera *Cibicidoides wuellerstorfi* (site MD96-2098), and (f) alkenone-derived SST (°C) off Lüderitz in the Benguela Upwelling System. Marine isotopic stages (MIS) boundaries are defined after LR04-Stack (Lisiecki and Raymo, 2005). Glacial stages 2 and 4 are indicated by the gray shadings (upper panel). The light-blue shading indicates the occurrence of the Last Glacial Maximum (LGM). Lower panel: the inverted red triangles represent the tie-points for MD96-2098 stratigraphy while the inverted dark gray triangles represent ^{14}C datings of GeoB3606-1 (Romero, 2010)

LGM (Fig. 3a). Minor peaks were observed at 52 kyr, 46–44 kyr, and 37,5–37 kyr. Lowest diatom$_{AR}$ ($<0.4 \times 10^9$ valves g^{-2} kyr^{-1}) occurred during the late MIS4, the MIS4/MIS3 transition, and from the deglaciation until ca. 6 kyr.

The diatom assemblage preserved in core MD96-2098 was highly diverse (number of species identified = ~40). The upwelling group (see 3.3.2.) dominated (>80 % of relative contribution) the total assemblage from 70 kyr until ca. 17 kyr, when the most important temporal switch in the species composition occurred (Fig. 4). Two rapid decreases in relative abundances of the upwelling group occurred at 57–55 kyr and 52–48 kyr.

Over the past 70 kyr, the contribution of pelagic–oligotrophic, benthic and coastal planktonic diatoms followed an inverse pattern than that of upwelling diatoms: contribution of the non-upwelling groups was high at 57–55 kyr and 52–48 kyr, and increased rapidly after 17 kyr into the mid Holocene. However, respective contributions showed different patterns during the considered intervals. The pelagic–oligotrophic group was dominant between 17 kyr and 10 kyr (deglaciation), while coastal planktonic diatoms were most abundant between 57–55 kyr and 52–48 kyr, and after 8 kyr until the late Holocene. Benthic diatoms were most abundant between 13 kyr and 8 kyr.

4.2. Bulk geochemical components

$CaCO_3$ was the dominant bulk biogenic component in MD96-2098 sediments, followed by opal and TOC. For the studied period, the content of $CaCO_3$ fluctuated between 21.1 % and 82.4 % (average = 42.4 %) (Fig. 3b). $CaCO_3$ had highest values between 16 kyr and 6.3 kyr. Secondary maxima occurred at 70–63 kyr, 55–50 kyr, and 45–38 kyr. Content of $CaCO_3$ was lowest in 64–60 kyr and 29–25 kyr. Opal values varied between 3.4 wt.% and 21.7 wt.% (average = 10.7 wt.%) (Fig. 3c) The greatest contribution of opal occurred between late MIS4 and early MIS3 (until ca. 42 kyr), and from mid MIS3 (37 kyr) through the late deglaciation (ca. 11 kyr). The relative content of TOC ranged from 0.9 wt.% to 6.2 wt.% (average = 4.2 wt.%) (Fig. 3d). TOC values remained above 4 wt.% between 61 kyr and ca. 15 kyr, with highest values occurring between 44 kyr and 15 kyr, and decreased abruptly afterward into the mid Holocene.

4.3. Benthic $\delta^{18}O$

The $\delta^{18}O$ record of the benthic foraminifera *C. wuellerstorfi* at site MD96-2098 exhibited substantial amplitude changes (~4.42 to 2.17 ‰, average 3.65 ± 0.57) (Fig. 3e). Isotopic values ranged from 4.1 ‰ to 3.1 ‰ between 65 kyr and 26 kyr. A moderate enrichment (3.79–4.39 ‰) occurred during the LGM. A decrease of almost 2 ‰ in $\delta^{18}O_{benthic}$ values is observed between late MIS2 and the mid Holocene.

4.4. Alkenone-derived SST

At the core site MD96-2098, for the interval 30.5–7 kyr, the low-resolution U^K_{37} record revealed an amplitude change of ca. 5 °C (range = 13.2–18.3 °C, average 15.2 ± 1.6 °C) (Fig. 3f). Lowest SSTs occurred between 28 kyr and 19 kyr. A warming of ca. 3 °C occurred around 15.5 kyr. Early Holocene SSTs remained above 17 °C.

The high-resolution U^K_{37} record of GeoB3606-1 showed that SSTs over the Lüderitz mid-slope were highly variable (range 12.0–18.1 °C, average 14.9 ± 1.5 °C), and recorded numerous substantial shifts throughout the past 70 kyr (Fig. 3f). The most prominent submillennial-scale shift of ~1–2 °C occurred between 70 kyr (late MIS4) and 45.5 kyr (mid MIS3). Lowest SST for the entire study interval occurred between 45 kyr and 40 kyr, followed by a rapid warming at 39–38 kyr. After the cooling at 37.5–34.5 kyr, submillennial-scale variations of SST persisted. SST increased by 3 °C from 34 kyr until 28.5 kyr. During the LGM, the SST presented small amplitude variations between 16.2 °C and 15.5 °C. A moderate cooling (16.4–16.6 °C) occurred

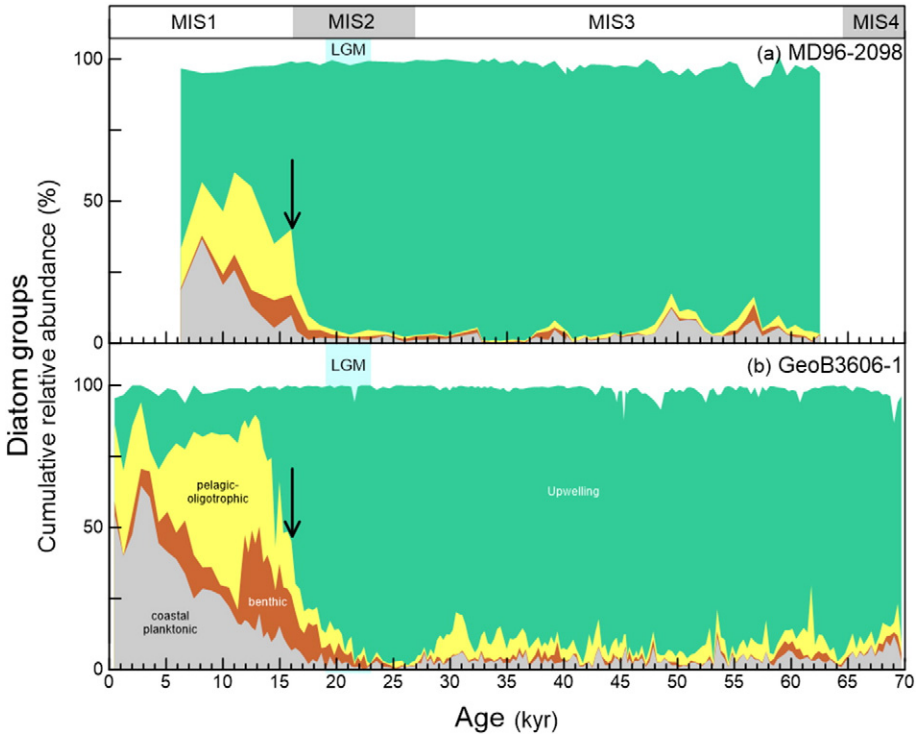

Fig. 4. Cumulative percentage (%) of four diatom groups (see 3.3.2.) in cores MD96-2098 (a; upper panel) and GeoB3606-1 (b; lower panel) off Lüderitz in the Benguela Upwelling System. References: upwelling (green), pelagic–oligotrophic (light yellow), benthic (brown), and light gray (coastal planktonic). Marine isotopic stages (MIS) boundaries are defined after LR04-Stack (Lisiecki and Raymo, 2005). Glacial stages 2 and 4 are indicated by the gray shadings (upper panel). The light-blue shading indicates the occurrence of the Last Glacial Maximum (LGM). The black arrow around 17 kyr defines the abrupt shift in the species composition of the diatom assemblage.

between 16 kyr and 14 kyr. For most of the Holocene, SST varied between 17.3 °C and 18.1 °C.

5. Discussion

We compared the records gained at the continental rise site MD96-2098 (water depth 2910 m) with those previously generated at the nearby site GeoB3606-1 (water depth 1785 m; Romero, 2010). This comparison allowed us to address the relationship between the location of the main diatom production center in frontal waters of the Lüderitz filament and the variability of upwelling intensity and Antarctic-derived Si at 25°–26°S off Namibia over the past 70 kyr.

5.1. Longitudinal expansions and contractions of the Lüderitz filament

Based on the knowledge that present-day primary productivity is enhanced at the filament front off Lüderitz and that frontal productivity forms a significant proportion of the total productivity of an upwelling cell (see above Section 2.), we argue that late Quaternary variations in productivity recorded in our sedimentary records allowed us to reconstruct past shifts in the front position. We propose that the seaward-shoreward (*i.e.* westward-eastward) migrations of the Lüderitz filament front at 25°–26°S occurred in four main phases as described below (Fig. 5).

5.1.1. Phase 1 (late MIS4 to mid MIS3, 70–44 kyr) — main upwelling front over the mid-slope off Lüderitz

Between 70 kyr and 44 kyr, lower values of diatoms, opal and TOC at site MD96-2098 than at site GeoB3606-1 (Fig. 3) suggested less intense upwelling and lower productivity in deeper pelagic waters than over the mid-slope off Lüderitz. Although the synchronous occurrence of upwelling over a large geographical area off Lüderitz is evidenced by the dominance of upwelling diatoms at both sites (Fig. 4), upwelling was more intense over site GeoB3606-1 than in waters overlying site MD96-2098. We primarily attribute the differences in siliceous primary paleoproductivity between the studied sites to the location of the outermost border of the Lüderitz filament, which was located closer to 13°E (GeoB3606-1) than to 12°E (MD96-2098) until around 44 kyr. Secondarily, the input of Si-rich waters above site GeoB3606-1 determined the highs and lows of diatom production.

5.1.2. Phase 2 (mid to late MIS 3, 44–31 kyr) — seaward displacement of the upwelling front

The increase of the total diatom concentration at site MD96-2098 around 38 kyr followed the decrease in diatom production (Fig. 3a, c, d) and the moderate increase of pelagic–oligotrophic taxa at site GeoB3606-1 around 44 kyr (Fig. 4). The diverse community of upwelling-related *Chaetoceros* spores also responded to the decreased availability of nutrients in waters overlying site GeoB3606-1 and switched from the dominance of high- to moderate-productive water spores (Romero, 2010).

5.1.3. Phase 3 (late MIS 3 to LGM, 31–19 kyr) — main upwelling front and diatom production center overlying deeper pelagial waters

The increase of diatom productivity at site MD96-2098 in the late MIS 3 (Figs. 3a, 6g) suggests the further seaward displacement of the outermost border of the upwelling front. No particular shift in the species composition of the diatom assemblage accompanied the diatom increase: *Chaetoceros* spores, typical of moderate upwelling intensity, dominated at site GeoB3606-1 throughout until ca. 20–19 kyr (Romero, 2010). This suggests that the hydrodynamic conditions for the occurrence of upwelling were present at both locations, though Si availability was higher over site MD96-2098 than over site GeoB3606-1.

5.1.4. Phase 4 (deglaciation to mid-Holocene, 19–6 kyr) — landward retraction of the Lüderitz filament

The distinctive shift in the species composition – from an upwelling-dominated to a non-upwelling community (Fig. 4) – and the increase of $CaCO_3$ values (Fig. 3b) occurred almost simultaneously at both sites during the early deglaciation. This evidence supports the scenario of the weakening of upwelling intensity over a broad part of the uppermost bathypelagial off Lüderitz, the landward retraction of the outermost border of the filament and the occurrence of Si-depleted waters.

5.2. Mechanisms and amplifiers responsible for the expansions and contractions of the Lüderitz filament

Since waters at the outermost front of the Lüderitz filament are colder and more productive than surrounding water masses (see 2.), rapid SST and diatom variations for the past 70 kyr off Lüderitz can be interpreted as recording the migrations of the filament front location and upwelling intensity. Mechanisms and amplifiers determining the seaward and shoreward migration of the outermost filament front off Lüderitz are discussed below.

5.2.1. Atmospheric and hydrographic forcing of the filament front migration and the diatom production off Lüderitz

The contractions and expansions of the Lüderitz filament mostly responded to Southern Hemisphere-driven atmospheric and hydrographic changes. The strength and the latitudinal position of the Southern Hemisphere westerlies and the concurrent extent of the subpolar gyres might have acted as a potential trigger for the forcing of the offshore streaming of the Lüderitz filament. The equatorward (poleward) expansion (contraction) of the Southern Hemisphere subtropical gyres (Peterson and Stramma, 1991; Beal et al., 2011) supply the mechanistic setting for the advection of warm Agulhas Water sourced from the Indian Ocean into the SE Atlantic Ocean. This transport might be an important step in initiating the frontal breakdown along the southern BUS (Lutjeharms and Stockton, 1987). Previous studies showed that the entrance of warm waters through the Indian-Atlantic Ocean Gateway – weak between late MIS 4 and late MIS 2 (Fig. 6a) – strongly influenced the hydrology of the southern BUS (Peeters et al., 2004; Beal et al., 2011). In support of this scenario, a numerical experiment based on a global general circulation model (Sijp and England, 2008) suggests that reduced leakage of Agulhas waters deprives the SE Atlantic of warm and saline Indian Ocean waters, leading to the cooling and freshening of waters in the southern BUS. Based on previous findings that the past position of the Southern Hemisphere westerlies exhibited natural decadal variability (Sijp and England, 2008; De Deckker et al., 2012) and that the hydrography around the southern tip of Africa has experienced strong millennial-scale variability (Peeters et al., 2004; Marino et al., 2013; Simon et al., 2013), we argue that the submillennial-scale coolings and warmings of alkenone-based SST at site GeoB3606-1 between 70 kyr and 27 kyr (Fig. 6e) responded to rapid contractions and expansions of the outermost front of the Lüderitz filament.

In addition to the teleconnections between the SE Atlantic and the subpolar gyres, the regional trade wind forcing along the Namibian coastal area at 25°–26°S might have amplified the sub-Milankovitch scale pattern of migration of the upwelling front location. Perennially consistent trade winds off Lüderitz (Shannon and Nelson, 1996) allow the almost year-around cooling and fertilization of surface waters of the Lüderitz filament (see above Section 2.). Sedimentological studies conducted on the upper slope core MD96-2087 (25.6°S, 13.38°E, 1029 m water depth) showed that the mean grain size of dust particles supplied to the ocean floor of the coastal SE Atlantic during the late Quaternary might be a reliable indicator of the aridity of the Namibian desert – the main dust source area for the study area – and of the wind strength in the neighboring Namibian upwelling (Fig. 6c; Pichevin et al., 2005b). The strong match between windier conditions and the overall trend of highest diatom values at site GeoB3606-1 from 65 kyr to 38 kyr is evidence of the

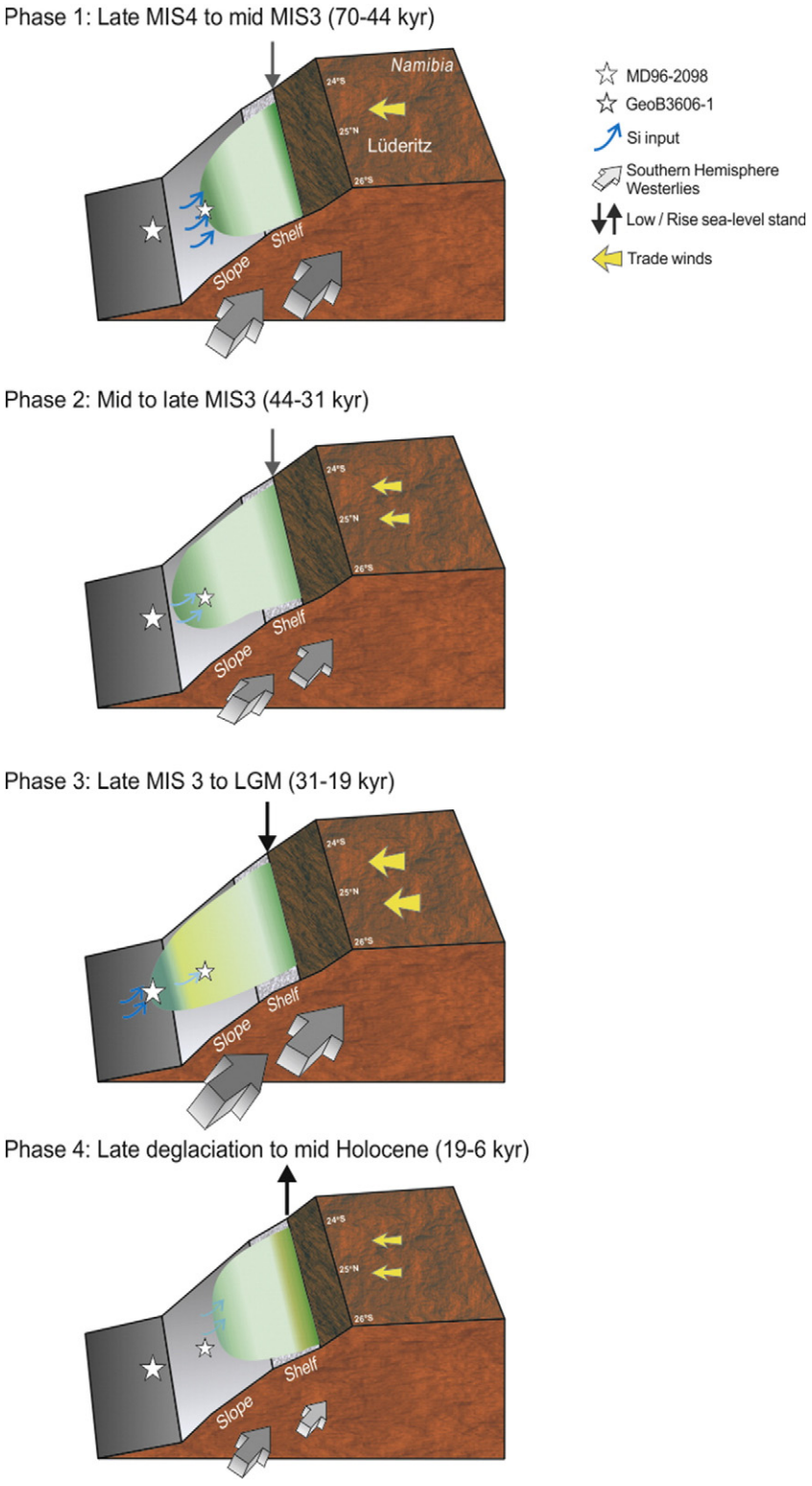

Fig. 5. Schematic representation of the four phases of changes of atmospheric and hydrographic features, sea-level stand and nutrient availability off Lüderitz during the past 70 kyr (left panel): (*1*) 70 kyr–44 kyr; (*2*) 44 kyr–31 kyr; (*3*) 31 kyr–19 kyr; and (*4*) 19 kyr–6 kyr. Right upper panel: large white star (site MD96-2098), small white star (GeoB3606-1), blue arrow (Si input), light gray arrow (Southern Hemisphere westerlies), black/gray arrows (sea level stand), and yellow arrow (trade winds). Different arrow thickness, and length and color darkness represent the strength of the mechanism discussed (larger/wider/darker = stronger, smaller/thinner/lighter = weaker). The areal cover of the Lüderitz filament is represented by the color-graded shading streaming offshore from the coastline (darker green tones represent higher productivity/more intense upwelling).

trade wind effect on the diatom production. Some mismatches between the SST record and the MD96-2087 wind record are possibly due to different sampling resolution (lower at site MD96-2087) and stratigraphic differences between both cores. Similarly, the increase of SST at both sites MD96-2087 and GeoB3606-1 (Fig. 6d, e) corresponds well the weakened trades intensity after 39 kyr (Fig. 6c, arrow).

The cooling between 23 and 19 kyr (Fig. 6d, e) was possibly due to more intense trade winds during the LGM (as evidenced by larger

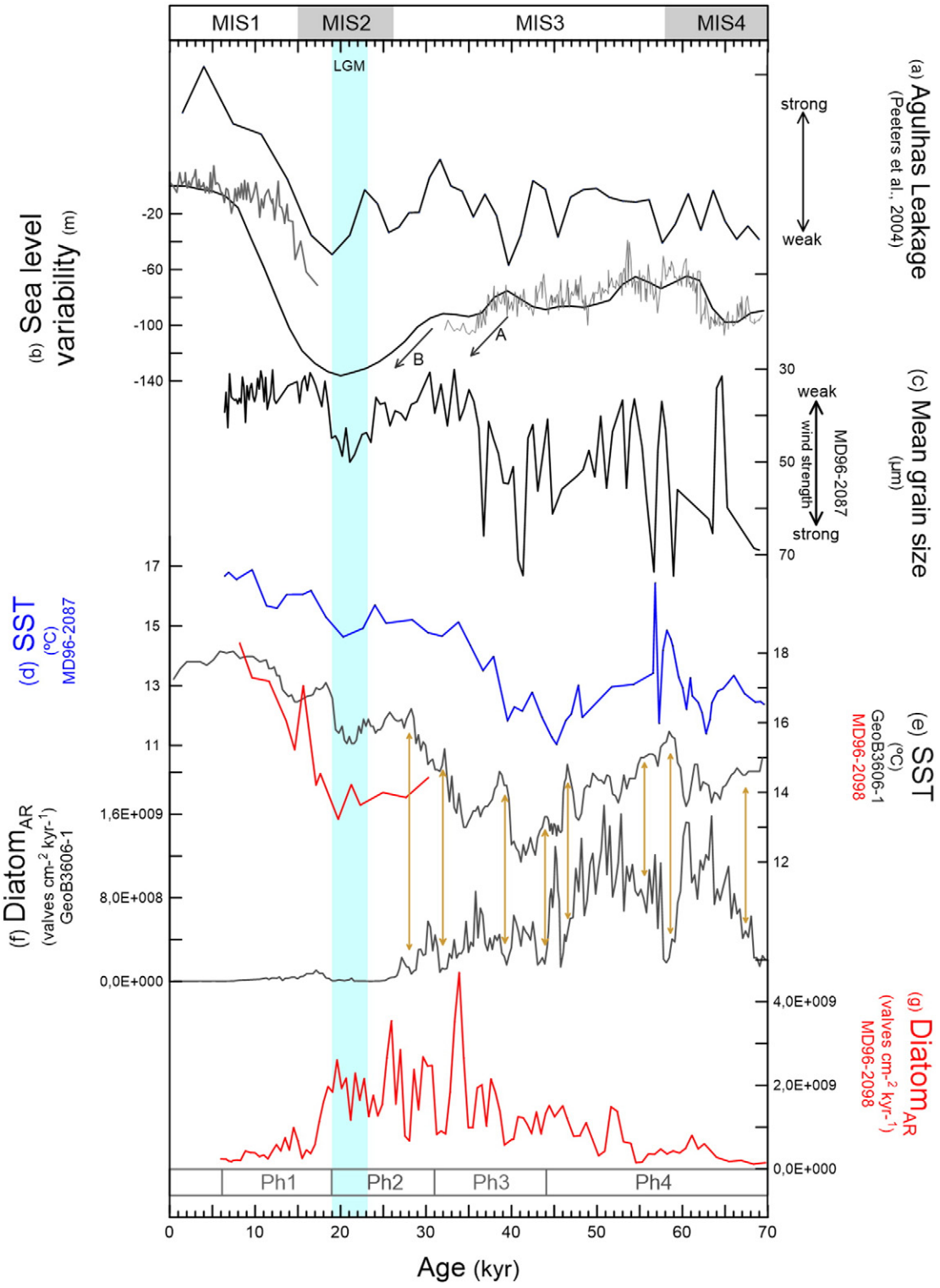

Fig. 6. Comparison of MD96-2098 and GeoB606-1 data with Agulhas Leakage, wind strength and global sea-level stand. (a) Agulhas leakage (represented by planktonic foramifera fauna from two cores in the Agulhas Basin, Peeters et al., 2004); (b) variability of sea level (m) (low resolution data, Waelbroeck et al., 2002; high resolution data, Rohling et al., 2009), (c) mean grain size (μm^{-2}, MD96-2087, Pichevin et al., 2005b), (d) SST (°C; MD96-2087, blue line, Pichevin et al., 2005b), (e) SST (°C; MD96-2098, red line, and GeoB3606-1, black line, this study), (f) total diatom$_{AR}$ (valves cm^{-2} kyr^{-1}, GeoB3606-1, black line; Romero, 2010), and (g) total diatom$_{AR}$ (valves cm^{-2} kyr^{-1}, MD96-2098, red line, this study). Black, single headed arrows A and B in (b) mark two-step rapid decreases of sea level stand. Light brown lines represent negatively correlated episodes of (e) SST GeoB3606-1 and (f) total diatom$_{AR}$ GeoB3606-1. Marine isotopic stages (MIS) boundaries are defined after LR04-Stack (Lisiecki and Raymo, 2005). Glacial stages 2 and 4 are indicated by the gray shadings (upper panel). The light-blue shading indicates the occurrence of the Last Glacial Maximum (LGM). Ph4 through Ph1 indicate the four phases of westward/eastward migration of the filament front off Lüderitz for the past 70 kyr (see also Fig. 5)

mean grain sizes between ca. 24 kyr and 19 kyr, Fig. 6c). In addition to the glacial equatorward shift of the Southern Hemisphere westerlies (Sijp and England, 2008), the stronger trades might have pushed the filament front beyond surface waters overlying site GeoB3606-1 further out into more open-ocean waters. Following strengthened winds, the increased mixing and the injection of cold thermocline waters into the

uppermost 20 to 40 m of the water column occurred over site MD96-2098 during the LGM, leading to high diatom production (Figs. 3a, 6g).

The simultaneous warming recorded along 25°–26°S during the last deglaciation (19–13 kyr) (Figs. 4e, 6d, e) provided a robust evidence for the shoreward retraction of the outermost border of the filament and the enhanced stratification of the uppermost water column over a large area off Lüderitz. This scenario is supported by the distinctive shift in the species composition of the diatom assemblage from an upwelling-dominated to a non-upwelling community over both study (Fig. 4), and the increase of $CaCO_3$ – indicative of increased calcareous productivity – values by the late MIS2 (Fig. 3b) that evidenced major changes in nutrient availability off Lüderitz. During the last deglaciation, the Southern Hemisphere westerlies weakened (Sijp and England, 2008) and the expansion of the gateway between southern Africa and the Southern Hemisphere Subtropical Front allowed increased leakage of Agulhas waters into the southern BUS (Fig. 6a; Peeters et al., 2004), which contributed to the warming of surface waters off Lüderitz.

5.2.2. Sea-level variations as a potential amplifier of the filament front migration

Sea level variations have been put forth as a possible explanation of variations of filaments fertility in low-latitude coastal upwelling areas (Bertrand et al., 2000; Giraud and Paul, 2010). Four main intervals of sea level fluctuations with magnitudes between −10 m and −120 m correspond with the time window covered by cores GeoB3606-1 and MD96-2098 (Fig. 6b). The interval of highest diatom values at site GeoB3606-1 between 68 kyr and 44 kyr matches a sea-level stand of 60 to 90 m lower than today. This lowering of the Namibian coastline contributed to displace the filament front closer to site GeoB3606-1 (Fig. 5), where upwelling rapidly varied between silica-rich and silica-depleted stages (see below Section 5.2.3.).

The second interval of sea level low-stand started around 44 kyr with a two-step decrease (Fig. 6b, arrows A and B). This decrease was concurrent with the increase of SST at core MD96-2087 (Fig. 6d) suggesting that the further lowering of sea level pushed the outermost filament seaward. Despite the fact that SST data for core GeoB3606-1 have higher resolution than those for the shallower MD96-2087, the overall pattern of temperature oscillations matches well between both localities (Fig. 6d, e), this being good indicator of the longitudinal migration of the filament front. Siddall et al. (2008) stated, however, that rapid sea level changes during MIS 3 might not have followed systematic, repeating patterns. We do not argue here that the millennial-to-submillennial SST variability at GeoB3606-1 fully followed the rapid sea level variations, but rather that the timing of sea level fluctuations amplified the intensity of upwelling determined by atmospheric and hydrological changes in the southern BUS.

During the LGM low-stand (third sea level interval), the Namibian coastline position lowered again by many tens of kilometers (Fig. 5), which might have acted as an amplifier by shifting the outermost front of the Lüderitz filament further out upon the pelagic realm. The lowest sea level stand, that exposed large areas close to the coastal environment during the LGM, did not compensate for the decrease induced by the reduced subsurface nutrient concentration over site GeoB3606-1.

Because of the sea level change along the Namibian coast after the LGM (Fig. 6b), it is tempting to argue that the rise of sea level during the last deglaciation shifted the filament front location closer to the Namibian coastline. Both study sites GeoB3606-1 and MD96-2098 were not in the same position relative to the maximum production center of the filament front upwelling, which became closer to closer to the Namibian coastline.

5.2.3. Availability of Antarctic-leaked Si off Lüderitz

Several short intervals of total diatom maxima matched marked sea surface coolings over the upper- (MD96-2087) and mid-slope (GeoB3606-1) off Lüderitz between 70 kyr and 27 kyr (Fig. 6d, e). On the other hand, episodes of diatom minima – dominated also by upwelling species (Fig. 4) – matched moderate-to-high SST (Fig. 6d, f). SST coolings and strong mixing of the uppermost water column alone cannot fully explain variations in total diatom concentration and shifts in the species composition. We postulate that changes in the Si content of BUS surface waters determined the occurrence of two types of upwelling off Lüderitz: silicate-rich *vs.* silicate-poor.

The occurrence of the Antarctic diatom *Fragilariopsis kerguelensis* in sediments of the southern BUS has been proposed to trace the advection of Si-rich, Antarctic-originated waters into the low-latitude SE Atlantic (Romero, 2010). Between 70 kyr and ca. 30 kyr, the inverse correlation between the relative abundance of *F. kerguelensis* (Romero, 2010) and the SST variations (*i.e.* highest *F. kerguelensis* values matched lowest SST) at the millennial scale suggested high availability of dissolved Si in upwelling waters. We postulate that intermittent pulses of Si into the BUS led to the upwelling of Si-rich waters. This nutrient scenario was triggered by the equatorward transport of Si-enriched waters of Antarctic origin, either by direct mixing or by the advection of Subantarctic Mode Waters (whose present-day Si content is low relative to surrounding water masses; Matsumoto et al., 2002) that invaded the middle to lower thermocline of subtropical coastal upwelling areas (Sarmiento et al., 2004). The equatorward leakage of dissolved Si followed intervals of lowered diatom productivity in the Southern Ocean south of the Subantarctic Front due of varying physical and biological conditions (sea ice cover, winds, Fe input) (Matsumoto et al., 2014). Two possible drawbacks of this sub-Milankovitch scale leakage scenario are the lack of a diatom reconstruction south of the Subantarctic Front showing millennial-scale variability, and the prediction of glacial increases and interglacial decreases of Si leakage (Brzezinski et al., 2002; Bradtmiller et al., 2009). In addition to bioavailable Fe fertilization (Brzezinski et al., 2002; Matsumoto et al., 2002), a recent model simulation experiment suggested that sea ice cover and the intensity of subpolar southern westerlies can also trigger the equatorward leakage of Si and that the biogeochemical response to each of the three triggers – not mutually exclusive – is different (Matsumoto et al., 2014). Additional evidence for a non-glacial, sub-Milankovitch Si leakage is provided by increased opal burial recorded in the eastern equatorial Pacific between 40 and 60 kyr, attributed to extended sea ice around Antarctica (Kienast et al., 2006). The diatom maxima at MD96-2098 during the MIS 3/2 transition and the LGM followed the leaked Si due to limited diatom production south of the Polar Front (Chase et al., 2003) as a consequence of the widely extended sea ice cover between ca. 25 kyr and 18 kyr (Crosta et al., 2005). The further lowering of the sea level around 27 kyr (Fig. 6b, arrow B, see Discussion above) might have amplified this signal by pushing the outermost border of the Lüderitz filament closer to MD96-2098.

The decreased Si delivery into the SE Atlantic after 19 kyr led to the almost simultaneous floral shift at both MD96-2098 and GeoB3606-1. Calcite-secreting coccolithophorids became dominant at the expense of silica-bearing diatoms. Higher $CaCO_3$ (lower opal) values at both sites from late MIS2 to the mid/late Holocene (Fig. 5b, c) indicated a shift in predominant nutrients toward Si-depleted waters over a wide area off Lüderitz. Following the lessened sea ice cover (Crosta et al., 2005), and the lowered input of Fe south of the Polar Front due to weakened wind intensity during the last deglaciation (Kohfeld et al., 2005; Sijp and England, 2008), Si was mainly consumed in waters south of the Subantarctic Front and became mostly trapped in underlying sediments (Brzezinski et al., 2002; Matsumoto et al., 2002). This scenario corresponds to the present-day dynamics of production and sedimentation of biogenic particulates in the southern BUS (Romero et al., 2002; Romero and Armand, 2010), where coccolithophorids dominate primary production over diatoms.

6. Conclusions

Based on the knowledge that present-day productivity is at its highest at the filament front, we reconstruct past variations of front

location off Namibia. Multi-parameter lines of evidences from this study suggest that several mechanisms and amplifiers determined the extension/contraction of the upwelling filament and the geographical location of the diatom production center off Lüderitz over the past 70 kyr. Atmospheric (wind intensity) and hydrographic/physical variability (surface and thermocline waters, SST and surface stratification, sea level stand), and nutrient supply (Si input) determined the settings for upwelling intensity and diatom production off Lüderitz. These mechanisms and amplifiers might have been linked and not been mutually exclusive.

The discussed mechanisms and amplifiers responsible for the strong diatom and SST fluctuations imply that the one-dimensional view of upwelling dynamics (downward flux of biogenic material from the surface balanced by upwelling of dissolved inorganic nutrients driven by vertical mixing of the thermocline) does not necessarily apply to the Lüderitz filament front.

The interpretation of the sedimentary signal as a record of regional conditions cannot be extrapolated to the entire BUS. Although our various proxies agree on details of the reconstructed sub-Milankovitch time scale variations, some ambiguities still remain to be explained. In this regard, further advances concerning mechanisms and amplifiers discussed here should be included in numerical modelizations of abrupt fluctuations of productivity and SST changes in low-latitude coastal upwelling systems. In particular, the possible impact of millennial-to-submillennial sea level changes, nutrient supply and sources, wind strength and their effect on productivity and CO_2 content for the past 70 kyr should be tested in the future.

Acknowledgements

Mr. J. Villanueva performed the U^K_{37} measurements on MD96-2098 (EPOC, Talence, France). OER was partially supported by the German Research Foundation (DFG). The research leading to these results has received funding from the European Research Council under the European Union's Seventh Framework Program (FP7/2007-2013)/ERC grant agreement n° [226600], which financed J.H.K. Comments and suggestions by two anonymous reviewers greatly improved a first version of this work. Data are available in the database www.pangaea.de.

References

Beal, L.M., De Ruijter, W.P.M., Biastoch, A., Zahn, R., 2011. On the role of the Agulhas system in ocean circulation and climate. Nature 472, 429–436.
Bertaux, J., Frohlich, F., Ildefonse, P., 1998. Multicomponent analysis of FTIR spectra: quantification of amorphous and crystallized mineral phases in synthetic and natural sediments. J. Sediment. Res. 68, 440–447.
Bertrand, P., 1997. NAUSICAA — Images II MD 105 Cruise Report. Institut Français pour la Recherche et la Technologie Polaire (IFRTP), Plocuzané, France, pp. 1–381.
Bertrand, P., Pedersen, T.F., Martinez, P., Calvert, S., Shimmield, G., 2000. Sea level impact on nutrient cycling in coastal upwelling areas during deglaciation: evidence from nitrogen isotopes. Glob. Biogeochem. Cycles 14, 341–355.
Bradtmiller, L.I., Anderson, R.F., Fleisher, M.Q., Burckle, L.H., 2009. Comparing glacial and Holocene opal fluxes in the Pacific sector of the Southern Ocean. Paleoceanography 24, PA2214. http://dx.doi.org/10.1029/2008PA001693.
Brzezinski, M.A., Pride, C.J., Sigman, D.M., Sarmiento, J.L., Matsumoto, K., Gruber, N., Rau, G.H., Coale, K.H., 2002. A switch from $Si(OH)_4$ to NO_3 depletion in the glacial Southern Ocean. Geophys. Res. Lett. 29. http://dx.doi.org/10.1029/2001GL014349.
Chase, Z., Anderson, R.F., Fleisher, M.Q., Kubik, P.W., 2003. Accumulation of biogenic and lithogenic material in the Pacific sector of the Southern Ocean during the past 40,000 years. Deep-Sea Res. II 50, 799–832.
Crosta, X., Koç, N., 2007. Diatoms: from micropaleontology to isotope geochemistry. In: Hilaire-Marcel, C., de Vernal, A. (Eds.), Proxies in Late Cenozoic Paleoceanography, Developments in Marine Geology Series. vol. 1. Elsevier, Amsterdam, The Netherlands, pp. 327–369.
Crosta, X., Shemesh, A., Etourneau, J., Yam, R., Billy, I., Pichon, J.J., 2005. Nutrient cycling in the Indian sector of the Southern Ocean over the last 50,000 years. Glob. Biogeochem. Cycles 19. http://dx.doi.org/10.1029/2004GB002344.
Crosta, X., Romero, O.E., Schneider, R., Ther, O., 2012. Climatically-controlled siliceous productivity in the eastern Gulf of Guinea during the last 40,000 years. Clim. Past 8, 415–431.
De Deckker, P., Moros, M., Perner, K., Jansen, E., 2012. Influence of the tropics and southern westerlies on glacial interhemispheric asymmetry. Nat. Geosci. 5, 266–269.
Giraud, X., Paul, A., 2010. Interpretation of the paleo–primary production record in the NW African coastal upwelling system as potentially biased by sea level change. Paleoceanography 25, PA4224. http://dx.doi.org/10.1029/2009PA001795.
Hasle, G.R., Syversten, E.E., 1997. Marine diatoms. In: Tomas, C.R. (Ed.), Identifying Marine Diatoms and Dinoflagellates. Academic Press, San Diego, USA, pp. 5–385.
Kienast, S.S., Kienast, M., Jaccard, S., Calvert, S.E., François, R., 2006. Testing the silica leakage hypothesis with sedimentary opal records from the eastern equatorial Pacific over the last 150 kyrs. Geophys. Res. Lett. 33, L15607. http://dx.doi.org/10.1029/2006GL026651.
Kim, J.-H., Schneider, R.R., Müller, P.J., Wefer, G., 2002. Interhemispheric comparison of deglacial sea-surface temperature patterns in Atlantic eastern boundary currents. Earth Planet. Sci. Lett. 194, 383–393.
Kirst, G., Schneider, R.R., Mueller, P.J., von Storch, I., Wefer, G., 1999. Late Quaternary Temperature Variability in the Benguela Current System derived from Alkenones. Quat. Res. 52, 92–103.
Kohfeld, K.E., Le Quéré, C., Harrison, S.P., Anderson, R.F., 2005. Role of marine biology in glacial–interglacial CO_2 cycles. Science 308, 74–78.
Lisiecki, L.E., Raymo, M.E., 2005. A Pliocene–Pleistocene stack of 57 globally distributed benthic $\delta^{18}O$ records. Paleoceanography 20, PA1003. http://dx.doi.org/10.1029/2004PA001071.
Longhurst, A.L., Sathyendranath, S., Platt, T., Caverhill, C., 1995. An estimate of global primary production from satellite radiometer data. J. Plankton Res. 17, 1245–1271.
Lutjeharms, J.R.E., Meeuwis, J.M., 1987. The extent and variability of South-east Atlantic upwelling. S. Afr. J. Mar. Sci. 5, 51–62.
Lutjeharms, J.R.E., Stockton, P.K., 1987. Kinematics of the upwelling front off Southern Africa. S. Afr. J. Mar. Sci. 5, 35–49.
Marino, G., Zahn, R., Ziegler, M., Purcell, C., Knorr, G., Hall, I.R., Ziveri, P., Elderfield, H., 2013. Agulhas salt-leakage oscillations during abrupt climate changes of the Late Pleistocene. Paleoceanography 28 (3), 599–606. http://dx.doi.org/10.1002/palo.20038.
Matsumoto, K., Sarmiento, J.L., Brzezinski, M.A., 2002. Silicic acid leakage from the Southern Ocean: a possible explanation for glacial atmospheric pCO2. Global Biogeochem. Cycles 16. http://dx.doi.org/10.1029/2001GB001442.
Matsumoto, K., Chase, Z., Kohfeld, K., 2014. Different mechanisms of silicic acid leakage and their biogeochemical consequences. Paleoceanography 20, 238–254. http://dx.doi.org/10.1002/2013PA002588.
Mollenhauer, G., Schneider, R.R., Müller, P.J., Spieß, V., Wefer, G., 2002. Glacial/interglacial variability in the Benguela upwelling system: spatial distribution and budgets of organic carbon accumulation. Glob. Biogeochem. Cycles 16. http://dx.doi.org/10.1029/2001GB001466.
Moreno-Ruiz, J.L., Licea, S., 1994. Observations on the valve morphology of *Thalassionema nitzschioides* (Grunow) Hustedt. In: Marino, D., Montresori, M. (Eds.), Proceedings of the 13th Symposium on Living and Fossil Diatoms. Biopress Limited Publisher, Bristol, U.K., pp. 393–413.
Moreno-Ruiz, J.L., Licea, S., Santoyo, H., 1996. Diatomeas del Golfo de California. Universidad Autónoma de Baja California Sur, México, Mexico, pp. 1–203.
Müller, P., Kirst, G., Ruhland, G., von Storch, I., Rosell-Melé, A., 1998. Calibration of the alkenone paleotemperature index U^K_{37} based on core-tops from the eastern South Atlantic and the global ocean (60°N–60°S). Geochim. Cosmochim. Acta 62, 1757–1772.
Peeters, F.J.C., Acheson, R., Brummer, G.-J.A., de Ruijter, W.P.J., Schneider, R.R., Ganssen, G.M., Ufkes, E., Kroon, D., 2004. Vigorous exchange between the Indian and Atlantic oceans at the end of the past five glacial periods. Nature 430, 661–665.
Peterson, R.G., Stramma, L., 1991. Upper-level circulation in the South Atlantic Ocean. Prog. Oceanogr. 26, 1–73.
Pichevin, L., Martinez, P., Bertrand, P., Schneider, R.R., Giraudeau, J., 2005a. Nitrogen cycling on the Namibian shelf and slope over the last two climatic cycles: local and global forcings. Paleoceanography 20. http://dx.doi.org/10.1029/2004PA001001.
Pichevin, L., Cremer, M., Giraudeau, J., Bertrand, P., 2005b. A 190 kr record of lithogenic grain-size on the Namibian slope: forging a tigh link between past wind-strength and coastal upwelling dynamics. Mar. Geol. 218, 81–96.
Prahl, F.G., Wakeham, S.G., 1987. Calibration of unsaturation patterns in long-chain ketone compositions for paleotemperature assessment. Nature 330, 367–369.
Prahl, F.G., Muehlhausen, L.A., Zahnle, D.L., 1988. Further evaluation of long-chain alkenones as indicators of paleoceanographic conditions. Geochim. Cosmochim. Acta 52, 2303–2310.
Rathburn, A.E., Pichon, J.-J., Ayres, M.A., DeDeckker, P., 1997. Microfossil and stable-isotope evidence for changes in Late Holocene paleoproductivity and paleoceanographic conditions in the Prydz Bay region of Antarctica. Palaeogeogr. Palaeoclimatol. Palaeoecol. 131, 485–510.
Rohling, E., Grant, K., Bolshaw, M., Roberts, A.P., Siddall, M., Hemleben, C., Kucera, M., 2009. Antarctic temperature and global sea level closely coupled over the past five glacial cycles. Nat. Geosci. 2, 500–504.
Romero, O.E., 2010. Changes in style and intensity of production in the Southeastern Atlantic over the last 70,000 yr. Mar. Micropaleontol. 74, 15–28.
Romero, O.E., Armand, L.K., 2010. Marine diatoms as indicators of modern changes in oceanographic conditions. In: Smol, J.P., Stoermer, E.F. (Eds.), The Diatoms: Applications for the Environmental and Earth Sciences, 2nd ed. Cambridge University Press, U.K., pp. 373–400.
Romero, O.E., Boeckel, B., Donner, B., Lavik, G., Fischer, G., Wefer, G., 2002. Seasonal productivity dynamics in the pelagic central Benguela System inferred from the flux of carbonate and silicate organisms. J. Mar. Syst. 37, 259–278.
Romero, O.E., Armand, L.K., Crosta, X., Pichon, J.-J., 2005. The biogeography of major diatom taxa in Southern Ocean surface sediments: 3. Tropical/Subtropical species. Palaeogeogr. Palaeoclimatol. Palaeoecol. 223, 49–65.
Romero, O.E., Kim, J.-H., Donner, B., 2008. Submillennial-to-millennial variability of diatom production off Mauritania, NW Africa, during the last glacial cycle. Paleoceanography 23. http://dx.doi.org/10.1029/2008PA001601.

Romero, O.E., Leduc, G., Vidal, L., Fischer, G., 2011. Millennial variability and long-term changes of the diatom production in the eastern equatorial Pacific during the last glacial cycle. Paleoceanography 26. http://dx.doi.org/10.1029/2010PA002099.

Romero, O.E., Mohtadi, M., Helmke, P., Hebbeln, D., 2012. High interglacial diatom paleoproductivity in the western most Indo-Pacific Warm Pool during the past 130,000 years. Paleoceanography 27. http://dx.doi.org/10.1029/2012PA002299.

Sarmiento, J.L., Gruber, N., Brzezinski, M.A., Dunne, J.P., 2004. High-latitude controls of thermocline nutrients and low latitude biological productivity. Nature 427, 56–60.

Shannon, L.V., 1985. The Benguela Ecosystem. 1. Evolution of the Benguela, physical features and processes. In: Barnes, M. (Ed.), Oceanography and Marine Biology, An Annual Review 23. University Press, Aberdeen, U.K., pp. 105–182.

Shannon, L.V., Nelson, G., 1996. The Benguela: large scale features and processes and system variability. In: Wefer, G., Berger, W.H., Siedler, G., Webb, D.J. (Eds.), The South Atlantic: Present and Past Circulation. Springer Verlag, Berlin Heidelberg, Germany, pp. 163–210.

Shillington, F.A., 1998. The Benguela upwelling system off southwestern Africa. In: Robinson, A.R., Brink, K.H. (Eds.), The Sea. 11, pp. 583–604.

Siddall, M., Rohling, E.J., Thompson, W.G., Waelbroeck, C., 2008. Marine isotope stage 3 sea level fluctuations: data synthesis and new outlook. Rev. Geophys. 46, RG4003. http://dx.doi.org/10.1029/2007RG000226.

Sijp, W., England, M.H., 2008. The effect of a northward shift in the southern hemisphere westerlies on the global ocean. Prog. Oceanogr. 79, 1–19.

Simon, M.H., Arthur, K.L., Hall, I.R., Peeters, F.J.C., Loveday, B.R., Barker, S., Ziegler, M., Zahn, R., 2013. Millennial-scale Agulhas Current variability and its implications for salt-leakage through the Indian–Atlantic Ocean Gateway. Earth Planet. Sci. Lett. 383, 101–112.

Sundström, B.G., 1986. Ph.D. Thesis. The Marine Diatom Genus *Rhizosolenia*. Lund University, Lund, Sweden, pp. 1–117.

Villanueva, J., Grimalt, J.O., 1997. Gas chromatographic tuning of the U^{K}_{37} paleothermometer. Anal. Chem. 69, 3329–3332.

Waelbroeck, C., Labeyrie, L., Michel, E., Duplessy, J.C., McManus, J.F., Lambeck, K., Balbon, E., Labracherie, M., 2002. Sea-level and deep water temperature changes derived from benthic foraminifera isotopic records. Quat. Sci. Rev. 21, 295–305.